Journal of Neuroscience Research 93:1492–1506 (2015)

Synapsin Knockdown Is Associated With Decreased Neurite Outgrowth, Functional Synaptogenesis Impairment, and Fast High-Frequency Neurotransmitter Release

Oscar Brenes,[1,2]* Carlo Natale Giuseppe Giachello,[3] Anna Margherita Corradi,[4] Mirella Ghirardi,[1,5] and Pier Giorgio Montarolo[1,5]

[1]Department of Neuroscience, Section of Physiology, University of Turin, Turin, Italy
[2]Department of Physiology, School of Medicine, University of Costa Rica, San José, Costa Rica
[3]Faculty of Life Sciences, University of Manchester, Manchester, United Kingdom
[4]Department of Experimental Medicine, University of Genova, Genova, Italy
[5]National Institute of Neuroscience, Turin, Italy

Synapsins (Syns) are an evolutionarily conserved family of synaptic vesicle-associated proteins related to fine tuning of synaptic transmission. Studies with mammals have partially clarified the different roles of Syns; however, the presence of different genes and isoforms and the development of compensatory mechanisms hinder accurate data interpretation. Here, we use a simple in vitro monosynaptic *Helix* neuron connection, reproducing an in vivo physiological connection as a reliable experimental model to investigate the effects of Syn knockdown. Cells overexpressing an antisense construct against *Helix* Syn showed a time-dependent decrease of Syn immunostaining, confirming protein loss. At the morphological level, Syn-silenced cells showed a reduction in neurite linear outgrowth and branching and in the size and number of synaptic varicosities. Functionally, Syn-silenced cells presented a reduced ability to form synaptic connections; however, functional chemical synapses showed similar basal excitatory postsynaptic potentials and similar short-term plasticity paradigms. In addition, Syn-silenced cells presented faster neurotransmitter release and decreased postsynaptic response toward the end of long tetanic presynaptic stimulations, probably related to an impairment of the synaptic vesicle trafficking resulting from a different vesicle handling, with an increased readily releasable pool and a compromised reserve pool.

Key words: synapsins; invertebrates; synaptic transmission; synapses; neurites; NCBI taxonomic ID: 6535; RRID:nif-0000-00313; RRID:nif-0000-30467; RRID:AB_11181145; RRID:rid_000085; RRID:rid_000081

The transmission of information in the nervous system depends on proper formation and functioning of a complex array of neuronal circuits, processes that require a fine regulation of complex mechanisms (Washbourne et al., 2004). Deficiencies in processes such as neurite outgrowth, synapse formation, and neurotransmitter release have inevitable consequences for nervous system function, leading to development of behavioral and/or cognitive diseases.

The synapsins (Syns) are an evolutionarily conserved family of presynaptic vesicle-associated phosphoproteins that play a major role in the fine tuning of synapse function. Furthermore, Syn mutations in humans have been associated with different pathologies (Garcia et al., 2004; Cesca et al., 2010; Fassio et al., 2011; Greco et al., 2013; Corradi et al., 2014).

Depletion of SynI, SynII, or SynIII results in inhibition of formation and maintenance of synapses and aberrant neuritic outgrowth or impaired axonal differentiation (Ferreira et al., 1994, 1995, 1998, 2000). However, some

SIGNIFICANCE:

Synapsins (Syns) are a family of presynaptic proteins associated with several cellular processes, whose mutations have been associated with different pathologies. The characterization of the specific role of Syns in synapse establishment and function in simple models will help in understanding the genesis of these pathologies in more complex organisms. Using a monosynaptic model, this study highlights the relevant role of Syns in promoting neurite outgrowth and formation of functional synapses and in regulating the fine tuning of neurotransmitter release, modulating the size of the readily releasable pool of synaptic vesicles and the capacity to respond to high-frequency stimulation.

Contract grant sponsor: Italian Ministry of the University and Research PRIN 2009 Grants (to P.G.M); Contract grant sponsor: Compagnia di San Paolo (to P.G.M., M.G.).

*Correspondence to: Oscar Brenes. Department of Physiology, School of Medicine, University of Costa Rica, 2060 San José, Costa Rica. E-mail: oscar.brenes_g@ucr.ac.cr

Received 27 April 2015; Revised 25 June 2015; Accepted 9 July 2015

Published online 27 July 2015 in Wiley Online Library (wileyonlinelibrary.com). DOI: 10.1002/jnr.23624

aspects of their functional role in neuronal development are still controversial; it has been reported that SynI/II double deletion largely decreases the deleterious developmental effects of individual deletions (Ferreira et al., 1998), and knocking out all three Syn genes (TKO) results in cells presenting milder development impairments and no significant alterations in gross neuronal development (Gitler et al., 2004b; Cesca et al., 2010; Valtorta et al., 2011).

It is also well accepted that Syns influence synapse formation and act in the modulation of synaptic vesicle (SV) pools (Gaffield and Betz, 2007; Valtorta et al., 2011; Orenbuch et al., 2012). However, the exact function is still unclear, given that there are conflicting reports about the readily releasable pool (RRP) size (Gitler et al., 2004b; Kile et al., 2010; Farisello et al., 2013), the total number of SVs, and the amplitude of the excitatory postsynaptic currents (Feng et al., 2002; Gitler et al., 2004b; Chiappalone et al., 2009; Farisello et al., 2013; Medrihan et al., 2013) in TKO vs. wild-type (WT) mice.

The discrepancies among single-, double-, and triple-knockout (KO) models could reflect the development of compensatory mechanisms in mice lacking two or more Syns, hindering accurate data interpretation (Cesca et al., 2010). The lack of conditional TKO models, which could prevent developmental compensation, hampers the testing of this possibility in mammalian models. In addition, the presence of different genes and isoforms in mammalian Syns with overlapping functions interferes with their clear characterization. For these reasons, we decided to use an in vitro monosynaptic *Helix* neuron connection as a model to study Syn knockdown.

The land snail *Helix* provides several advantages because specific identifiable neurons can be isolated, and reliable connections can be formed in vitro, culturing physiological synapses that recapitulate in vivo features (Ghirardi et al., 1996; Fiumara et al., 2001, 2005), thereby avoiding nonspecific effects resulting from surrounding tissue or random connections. This model has been used in several studies addressing the effects of Syn phosphorylation on synapse function (Ghirardi et al., 1996; Fiumara et al., 2001, 2004, 2007; Giachello et al., 2010). *Helix* neurons provide a convenient genetic organization (Fiumara et al., 2007), a single Syn gene that can be blocked by antisenseRNA (asRNA) and also offers amenability to experimental manipulations such as plasmid intranuclear microinjection, allowing the constitutive expression of asRNAs in cells that can be coupled to their physiological target, permitting the silencing of Syn in specific monosynaptic circuits to study synapse properties.

MATERIALS AND METHODS

Materials

All chemicals and reagents used in this study were purchased from Sigma (Milan, Italy), unless stated otherwise.

Animals

Juvenile specimens of *Helix aspersa* land snails (NCBI Taxonomic ID: 6535) were provided by local breeders and maintained inactive at a temperature of 6°C. Before experimental procedures, snails were kept in an active state for at least 16 hr in a climate chamber, with temperature and humidity (20°C and 70%, respectively) regulated. During the activity period, snails were fed lettuce and water ad libitum. During surgical procedures, the snails were always anesthetized, and efforts were made to minimize the number and suffering of animals used, in accordance with Directive 2010/63/EU of the European Parliament and of the Council of 22 September 2010 on the protection of animals used for scientific purposes.

Cell Culture

Cell cultures were performed as previously described (Ghirardi et al., 1996). Briefly, snails were anesthetized by injection of isotonic $MgCl_2$ in the foot. Cerebral and buccal ganglia were surgically isolated and incubated for enzymatic digestion in protease type XIV in isotonic L15 medium (0.3 U/ml) at 34°C for 3–3.5 hr. After digestion, the ganglia were washed twice in L15 medium, and C1 and B2 neurons were individually isolated and identified by their position in the ganglia and their size. For experiments with cells plated with their axonal stumps, cells were gently isolated with the initial segment of their original axons still attached to somata and immediately plated on dishes pretreated with poly-L-lysine and *Aplysia* hemolymph. For experiments with axon-reabsorbed somata (soma configuration), neurons were isolated and transferred to dishes pretreated with 5% bovine serum albumin (BSA) to prevent cell–substrate adhesion, as previously described (Fiumara et al., 2005). After 24 hr, floating neurons retracted their processes, yielding spherical somata. Then, floating somata were gently manipulated according to the specific experimental protocols.

Plasmid Generation and Intranuclear Microinjection

The plasmid $pNEX_3$ containing EGFP sequence (pNEX-EGFP) was used as a control. Standard recombinant DNA techniques were used to insert the DNA sequence complementary to the 3′ one-third of mRNA of *Helix* Syn (helSyn; a fragment of 544 bp) in the $pNEX_3$ plasmid, depleted of EGFP (pNEX-helSynAS). Control cells were intranuclearly microinjected with the pNEX-EGFP alone, whereas knocked-down cells (helSynKD cells) were injected with both pNEX-helSynAS and pNEX-EGFP.

Intranuclear microinjection was performed with a glass electrode, with the tip filled with a solution containing the plasmids (1 μg/ml each), KCl (0.2 M), and fast green solution 0.2% (p/v); the cell was loaded by using short pressure pulses (10–20 pulses, 2–10 psi) delivered through a pneumatic picopump (PV820, WPI, Sarasota, FL) connected to the electrode holder. The injection procedure was monitored under visual and electrophysiological control and stopped when the nucleus was uniformly colored.

TABLE I. Primary Antibody Used

Antigen	Description of immunogen	Source, host species, clone	Dilution used
Helix Syn	OVA-conjugated peptide NH2-CGDLQ GEANEKEDPPNVG-COOH	InBios International, rabbit, polyclonal antibody (Ab105)	1:500

Measurement of Neurite Length and Branching

To measure neurite length, brightfield images of cultures were acquired in Image Pro Plus (Media Cybernetics, Bethesda, MD; RRID:nif-0000-00313) with a Monochrome Evolution QE camera (Media Cybernetics) at 24, 48, 72, and 96 hr after plating. The measurement of neurite length of cells plated with the initial segment of their original axons was performed on axonal extensions originating from the tip of the axonal stump. In soma configuration experiments, the measurement was performed on neurites that originated from the soma. At least 30 neurites per cell were measured in ImageJ 1.44 (NIH, Bethesda, MD; RRID:nif-0000-30467), and their linear elongation was followed in time. The quantification of total amount of neurite field was performed as previously described (Ghirardi et al., 1996). Briefly, concentric rings (at 25-μm intervals) with their center localized in the center of the soma were drawn, and the number of intersections with neurites was counted as a general indication of the neurite branching. When necessary, brightness and contrast were adjusted in the entire image.

Immunocytochemistry

Cultures were washed three times (10 min each) in *Helix* saline solution (NaCl 0.6 %) at room temperature (RT) and then fixed with 4% paraformaldehyde in 0.1 M phosphate-buffered saline (PBS; 45 min at RT). Afterward, cultures were rinsed in 0.01 M PBS and treated with blocking solution (5% BSA and 0.25% saponin in 0.01 M PBS) for 1 hr at RT. The cultures were then incubated overnight at 4°C with a rabbit anti-helSyn custom antibody (1:500 dilution; Table I) in blocking solution. After having been rinsed with 0.25% saponin in 0.01 M PBS, the cultures were incubated in blocking solution with an Alexa-conjugated anti-rabbit IgG (1:500 dilution; catalog No. A10040; RRID:AB_11181145; Life Technologies, Grand Island, NY) secondary antibody, and after 45 min at RT cultures were washed three times in 0.01 M PBS. Finally, cultures were kept in 0.1 M PBS, and cell images were captured with a Monochrome Evolution QE camera with an Eclipse TE200 inverted microscope (Nikon Instruments, Tokyo, Japan) equipped with epifluorescence optics.

Antibody Characterization

Table I shows the antibody against helSyn used in this study. The helSyn polyclonal antibody was manufactured by InBios International (Seattle, WA). OVA-conjugated peptide was used for the immunization of a rabbit, and the resultant affinity-purified polyclonal antibody Ab-105 was tested against free synthetic peptide by ELISA. Specificity of the custom-made antibody was tested by Western blotting over *Helix* ganglia lysate. The total level of helSyn (phosphorylated or non-phosphorylated) was revealed as a doublet with a molecular mass of approximately 28 kDa.

helSyn Quantification

Quantitative analysis of fluorescence was performed on areas of 50 × 50 μm, with an almost complete coverage of the neurite field. To quantify the presence of helSyn in cell varicosities, a radiometric imaging analysis, defined as targeting factor (TF), was performed as previously described (Gitler et al., 2004a). Briefly, cells were coinjected with the asRNA-generating plasmid (pNEX-helSynAS) and pNEX-EGFP. Fluorescence intensities of EGFP and Alexa-conjugated secondary antibody were measured independently (Fig. 1). Using the Line Profile tool of Image Pro Plus, we drew a line across the varicosities and the proximal neurites, obtaining a plot of the pixel intensity values for each wavelength, corrected for the measured local background values. The peak of fluorescence of the line profile represents varicosity intensity, whereas tails represent the proximal neurites. The ratio of intensities of fluorescence produced by the Alexa-conjugated antibody against helSyn antibody (SynAb) was corrected for variations in cell volume by using the ratio of fluorescence of the free diffusion dye EGFP, according to the following equation; thus, a decrease in the value of the targeting factor represents a reduction in helSyn protein: targeting factor = $([\text{varicosity}_{\text{SynAb}}/\text{neurite}_{\text{SynAb}}]/[\text{varicosity}_{\text{EGFP}}/\text{neurite}_{\text{EGFP}}]) - 1$.

Varicosity Analysis

A roughly spherical structure with an area of between 2 and 25 μm^2 was considered as a varicosity. Cell varicosities were counted manually by using micrographs of the whole neuritic field of each cell (×10). Varicosity areas were digitally measured on micrographs (×60) with an almost complete coverage of the neurite field. When necessary, brightness and contrast were adjusted in the entire micrograph.

Electrophysiological Recordings

Standard intracellular recording techniques were used on cultured cells under an Eclipse TE200 inverted microscope, as previously described (Fiumara et al., 2005, 2007). Briefly, the cells were impaled with glass intracellular electrodes filled with 2.5 M KCl (resistance ~10 MΩ). Signals were amplified by an Axoclamp 900A amplifier (Axon Instruments, Union City, CA) in current-clamp mode; digitally converted by means of a Digidata 1322A analog/digital converter (Axon Instruments); and monitored, recorded, and analyzed with pClamp software (Axon Instruments; RRID:rid_000085) with a personal computer. Specifically, signals were recorded with Axoscope software, and recorded traces were analyzed in Clampfit software.

Sniffer Detection of Neurotransmitter Release

The evaluation of neurotransmitter (NT) release from single C1 neurons was performed by using a freshly isolated 5-HT-sensitive B2 neuron from the *Helix* buccal ganglia as an assay cell sniffer (Fiumara et al., 2001; Ghirardi et al., 2001). We took particular care in the micromanipulation of the

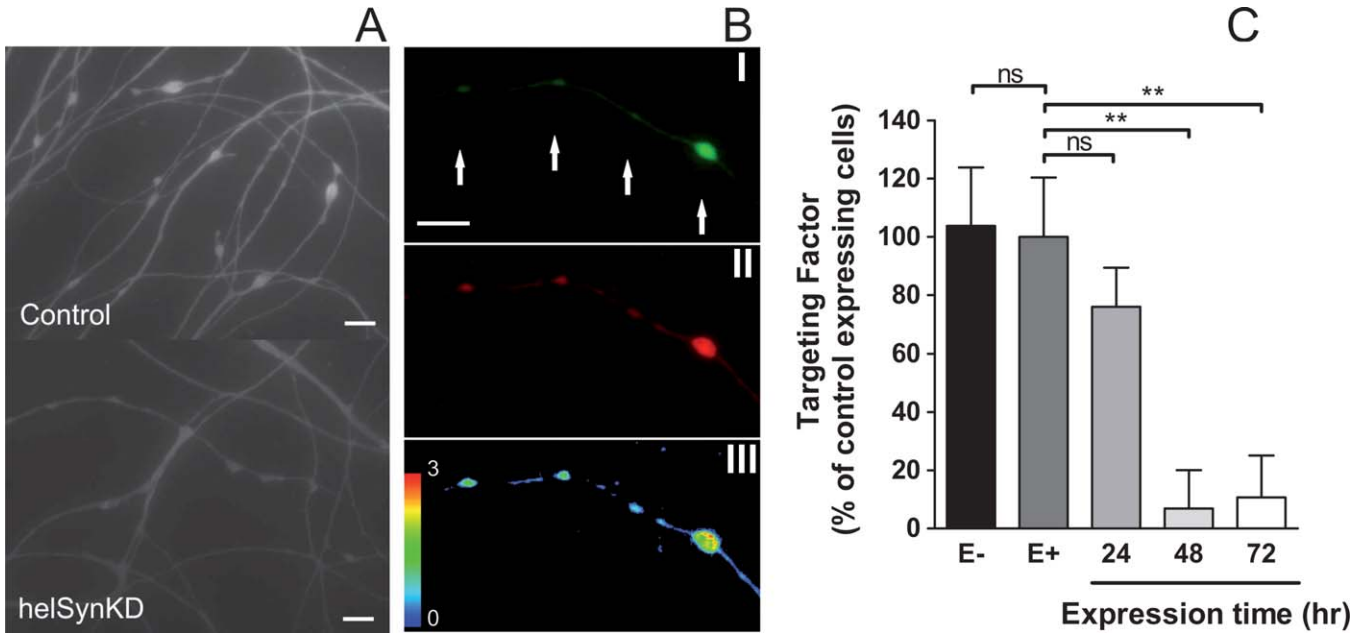

Fig. 1. *Helix* Syn knockdown by asRNA constitutive overexpression. **A:** Fluorescence micrographs of control and Syn-silenced cells (helSynKD) immunolabeled with a custom-made antibody against helSyn after 48 hr of expression. **B:** Quantification of helSyn by the fluorescence radiometric imaging analysis TF. Fluorescence intensity of EGFP (I) and helSyn immunostaining (II) were quantified for each varicosity and its proximal neurites, and then TF was calculated for each varicosity (III). **C:** helSyn protein expression was quantified by using the TF in cells expressing the asRNA for different time periods and in control cells expressing and not expressing EGFP (E^+ and E^-, respectively). Each bar indicates mean ± SEM. $^{**}P < 0.01$. Scale bars = 5 μm in A; 10 μm in B.

impaled sniffer cells above the neurite outgrowth spreading from the C1 neurons. The membrane potential of the B2 sniffer neuron was kept at –80 mV. The C1 neurons were intracellularly stimulated with depolarizing current pulses to fire a train of action potentials (10 Hz for 5 or 40 sec). The sniffer responds to the 5-HT released from the varicosities in the vicinity, and the amount of 5-HT released from the stimulated C1 neuron was estimated as the amplitude of the depolarization recorded from the sniffer neuron.

Assessment of Synaptic Connectivity and Plasticity

Connectivity and activity-dependent plasticity were analyzed, as previously described (Fiumara et al., 2005). The presence and the type (electrical vs. chemical) of synaptic connections between the paired C1 and B2 neurons were assessed by injecting hyperpolarizing or depolarizing currents into C1 neurons and analyzing the effect on the membrane potential of B2. Pairs were considered to be electrically coupled when the presynaptic injection of hyperpolarizing current (0.5 nA for 2 sec) caused detectable hyperpolarization in the follower cell (see Fig. 5B). The coupling rate was calculated as the ratio between postsynaptic and presynaptic membrane hyperpolarization amplitude. Pairs were considered to be chemically coupled when presynaptic action potentials (APs) evoked excitatory postsynaptic potentials (EPSPs) with a short delay (at least 5 msec) after the peak of the presynaptic AP (see Fig. 5B, dashed lines). In electrical–chemical mixed synapses, both transmissions occurred simultaneously, and presynaptic APs determined a two-phase postsynaptic response. Here, the two components can easily be distinguished by the synaptic delay and the relatively slow rise kinetic of the chemical C1–B2 connection (see Fig. 5B).

To investigate the activity-dependent plasticity, we used only chemically connected couples. Stimulations were delivered by intracellular injection of suprathreshold depolarizing current pulses (30 msec each), triggered by an S88 dual-output stimulator (Grass Technologies, Warwick, RI). During stimulation protocols, the basal membrane potential of the postsynaptic B2 neuron was kept hyperpolarized to –80 mV to prevent firing. Paired-pulse facilitation (PPF) was estimated as the ratio between two EPSPs evoked by two presynaptic APs with a 100- or a 500-msec interspike interval (ISI). Frequency facilitation (FF) was evoked with five pulses at 2 Hz, and it was estimated as the ratio of the fifth EPSP with respect to the first one. To induce posttetanic potentiation (PTP), the presynaptic neuron was stimulated to fire at a basal rate of 0.05 Hz (basal stimulation); after five APs, a 2-sec tetanic stimulation (10 Hz) was applied, and 0.05-Hz stimulation was resumed 30 sec after the end of the train. For statistical comparisons, the amplitude of the posttrain EPSPs was normalized to the mean amplitude of the five pretrain EPSPs.

Estimate of the RRP of Synchronous Release Size

The size of the RRP of synchronous release (RRP_{syn}) was calculated by using the cumulative amplitude analysis (Schneggenburger et al., 1999, 2002). C1 neurons were

stimulated by a train (10 Hz for 10 sec), and the RRP_{syn} was determined by summing peak EPSP amplitudes during the first 50 repetitive stimuli. During this depleting stimulus, the EPSPs declined and reached a steady state, typically interpreted as the ongoing replenishment of the depleted RRP (Schneggenburger et al., 1999). The number of data points to include in the linear fitting of the steady-state phase was evaluated by calculating the best linear fit, including the maximal number of data points starting from the last (see Fig. 7E). The best linear fit was then back extrapolated to time 0, and the interception with the y-axis was used as an estimate of the size of the RRP_{syn}, expressed in mV. The slope of the regression line provided an indicator of the rate of vesicle replenishment. EPSPs of the first 5 sec of tetanus were also normalized against the first EPSP of the train and plotted as a function of time to appreciate better the ratio of each EPSP with respect to the first one.

Statistical Analysis

Data are expressed as mean ± SEM. Statistical analysis was performed in Prism 5 (GraphPad Software, San Diego, CA; RRID:rid_000081). Statistical significance between two or more groups was assessed by Fisher's exact (FE) test, two-tailed Student's *t*-test (normal or Welch's corrected, when appropriate), or ANOVA (one- or two-way, when appropriate), followed by the Bonferroni post hoc test. Significance level was set at $P < 0.05$.

RESULTS

Quantification of helSyn Targeting and Knockdown

Different immunocytochemical studies have demonstrated that Syn isoforms are distributed in a punctate pattern along neurites, and there are differences in the targeting properties of the various Syn isoforms, according to the specific structural domain composition. Similarly to mammalian orthologous, the punctate distribution of helSyn has been observed in intact central nervous system (Ghirardi et al., 1996) and in isolated cultured cells (Ghirardi et al., 1996; Fiumara et al., 2007; Giachello et al., 2010, 2013).

As previously observed, when the serotonergic C1 neuron of *Helix* snail was used, immunocytochemical staining showed a punctate distribution in helSyn, localized predominantly in varicosities along neurites (Fig. 1A,B). However, to measure helSyn protein expression levels in varicosities precisely, the immunostaining intensity alone is not an appropriate measure because this value is affected by the volume of the cellular compartments. For this reason, we decided to use a ratiometric imaging method called TF (Gitler et al., 2004a). Cells were microinjected with a plasmid codifying for EGFP (pNEX-EGFP), a free-diffusion dye that allowed us to visualize the volume of cellular compartments (Fig. 1BI, green signal), and then helSyn distribution was estimated by anti-helSyn antibody immunofluorescence analysis (Fig. 1BII, red signal). Fluorescence intensity of both signals (helSyn and EGFP) was quantified on identified varicosities and on its adjacent neurite segments, and subsequently the TF was estimated (Fig. 1BIII). For single C1 *Helix* neurons (n = 12), we obtained a helSyn TF of 0.32 ± 0.04, confirming its positive targeting to the varicose structures. Similar TF values have been reported for human Syn isoforms, such as hSynIb (Gitler et al., 2004a).

TF was subsequently used to quantify time-dependent changes in helSyn expression level during asRNA overexpression (Fig. 1A). We found no difference in the immunostaining intensity of helSyn between cells expressing EGFP (n = 9) and injected cells that did not express EGFP (n = 10; $P > 0.05$). Conversely, when cells were coinjected with pNEX-EGFP and pNEX-helSynAS, the antisense expression correlated with a time-dependent reduction in the amount of helSyn staining ($F_{4,36} = 7.52$, $P = 0.0002$, one-way ANOVA), confirming significant protein loss after 48 hr (6.92% of control value; n = 9; $P < 0.01$, Bonferroni's multiple-comparisons post hoc test) and 72 hr (10.67% of control value; n = 7; $P < 0.01$, Bonferroni's multiple-comparisons post hoc test) following asRNA expression.

Impairment in Neurite Linear Outgrowth, Branching, and Varicosity Formation Resulting From helSyn Knockdown

Because there are conflicting reports of Syn roles in neurite outgrowth among single-, double-, and triple-KO mouse models (Ferreira et al., 1994, 1995, 1998, 2000; Gitler et al., 2004b; Cesca et al., 2010; Valtorta et al., 2011), we analyzed the effects of *Helix* Syn knockdown on neurite linear outgrowth and branching. To analyze linear outgrowth, we used two starting conditions. In the first case (Fig. 2A–C), cells were isolated and plated with the initial segment of their original axons. After attachment, cells were microinjected with the plasmids, and neurite growth was determined every 24 hr and normalized against the growth of control cells at the moment when asRNA expression was visually confirmed (T0 as 100%). helSynKD cells (n = 7) showed a significant slowdown in neurite outgrowth after asRNA expression was confirmed vs. control cells (n = 6; treatment $F_{1,46} = 53.36$, $P < 0.0001$; time $F_{4,46} = 81.70$, $P < 0.0001$; and interaction $F_{4,46} = 7.74$, $P = 0.0001$, two-way ANOVA). After the beginning of asRNA expression, the neurites appeared 33.1% shorter at 24 hr ($P < 0.01$, Bonferroni's post hoc test), 43.0% shorter at 48 hr ($P < 0.001$, Bonferroni's post hoc test), and 47.5% shorter at 72 hr ($P < 0.001$, Bonferroni's post hoc test) compared with control cells.

For the second condition, to appreciate better the effect of Syn silencing, we used cells in soma configuration (Fiumara et al., 2005); cells were microinjected, kept in suspension, and plated 24 hr after the start of asRNA expression (Fig. 2D–F). In this configuration, the decrease in neurite linear outgrowth of Syn-silenced cells (n = 13) compared with controls (n = 12) was more pronounced (treatment $F_{1,78} = 250.4$, $P < 0.0001$; time $F_{3,78} = 112.9$, $P < 0.0001$; and interaction $F_{3,78} = 37.79$, $P < 0.0001$, two-way ANOVA). helSynKD cells showed reductions in the neurite outgrowth of 80.3% at 24 hr ($P < 0.001$, Bonferroni's post hoc test), 76.7% at 48 hr ($P < 0.001$, Bonferroni's post hoc test), and 70.6% at 72 hr ($P < 0.001$, Bonferroni's post hoc test) compared with control cells.

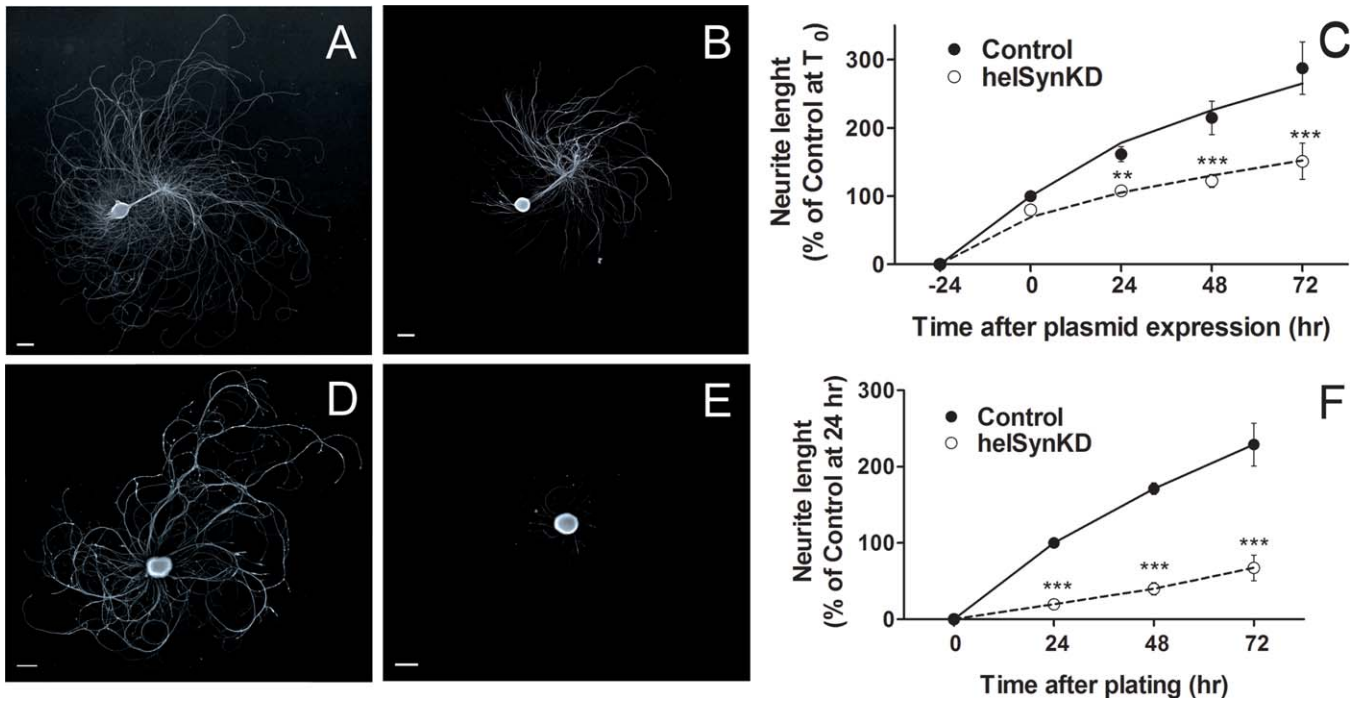

Fig. 2. Neurite outgrowth impairment after helSyn knockdown. Neurite outgrowth was analyzed in C1 neurons plated with the initial segment of their axons (**A–C**) and in C1 neurons plated as axon-reabsorbed somata (soma configuration; **D–F**). In C, control cells (solid circles) and Syn-silenced cells (helSynKD; open circles) were normalized to the control mean value measured at the moment when plasmid expression was visually confirmed (T0). In F, cells were plated 24 hr after plasmid expression started, and neurite outgrowth was normalized to the control mean value measured at 24 hr of plating. Each time point represents mean ± SEM. $^{**}P < 0.01$, $^{***}P < 0.001$. Scale bars = 100 μm.

Furthermore, the knocking down of helSyn had a profound effect on the branching of newly sprouting neurites. Beginning 48 hr after plating, the neuritic field of the helSynKD cells (n = 13) showed a strong reduction vs. control cells (n = 8; treatment $F_{1,190} = 32.90$, $P < 0.0001$; distance $F_{10,190} = 18.24$, $P < 0.0001$; and interaction $F_{10,190} = 11.84$, $P < 0.0001$, two-way ANOVA; Fig. 3).

In addition, downregulation of helSyn revealed a marked decrease in the total number of varicosities vs. control cells. When cells were plated with the initial segment of their original axons, there was a 40.70% decrease in the number of varicosities vs. control cells (100.00 ± 6.15% [n = 7] in control cells vs. 59.30 ± 5.60% [n = 10] in helSynKD cells; $t_{15} = 4.82$, $P < 0.001$). In soma configuration, we observed a stronger impairment in the formation of varicosities, with an 84.64% decrease in helSynKD cells (n = 14) vs. control cells (n = 10; $t_{22} = 5.46$, $P < 0.0001$; Fig. 4A). The area of the varicosities generated was also measured, with varicosities 38.96% smaller in helSynKD cells (n = 9) vs. control cells (n = 10; $t_{17} = 3.74$, $P = 0.0016$) in soma configuration (Fig. 4B). A small decrease (10.49%) was also observed when cells were plated with their axon; however, with this condition, the difference was not statistically significant ($P = 0.18$, *t*-test).

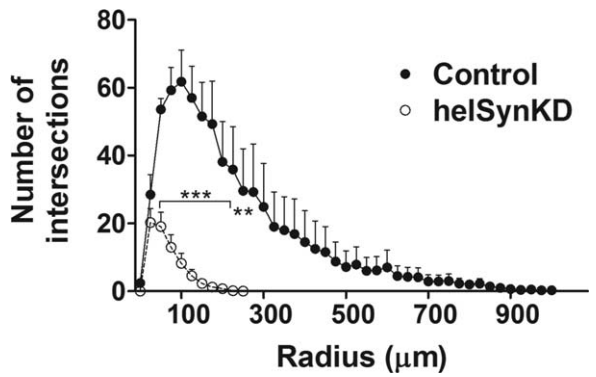

Fig. 3. Neuritic field decrease in Syn-silenced cells. The branching of neurites was estimated by counting the number of neurite intersections with concentric rings at intervals of 25 μm. Control cells (solid circles) developed neuritic fields with longer neurites and a higher number of branches than cells in which Syn was silenced (helSynKD; open circles). Each time point represents mean ± SEM. $^{**}P < 0.01$, $^{***}P < 0.001$.

helSyn Silencing Evoked Increased Neurotransmitter Release From Single C1 Somata During Short Tetanic Stimulations

Serotonin release from isolated C1 neurons was detected by using B2 neurons, one of its physiological

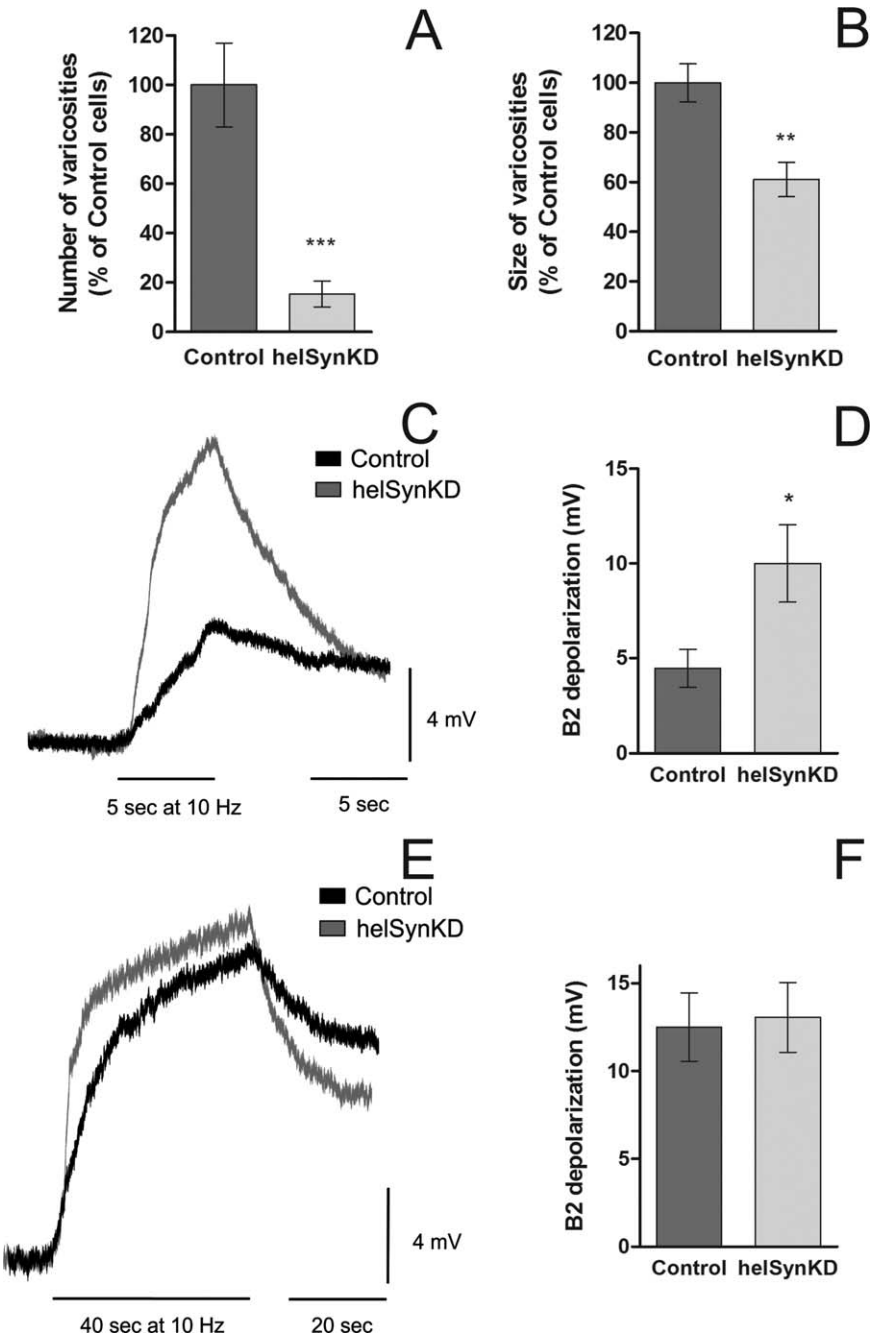

Fig. 4. Impairment in varicosity formation and increased neurotransmitter release in helSynKD cells. Cell varicosities were counted from micrographs of the whole neurite field of each cell in soma configuration (×10) and measured in micrographs with ×60. asRNA expressing cells (helSynKD) show a smaller number of varicosities along neurites (**A**) and a smaller mean size of the newly formed varicosities (**B**). Neurotransmitter release induced by a train of action potentials (horizontal bars in C and E) in C1 control and helSynKD cells was estimated as the mean depolarization in a B2 sniffer cell. The 5-sec train (**C,D**) shows an increased sniffer depolarization amplitude when helSynKD cells are stimulated. A 40-sec train induced similar depolarization amplitudes (**E,F**). Values represent mean ± SEM. $\star P < 0.05$, $\star\star P < 0.01$, $\star\star\star P < 0.001$.

targets. Freshly dissociated B2 neurons (sniffer) were micromanipulated in contact with the neuritic arbor of the C1 neurons. Neurotransmitter release was evoked by electrical stimulation of C1 at 10 Hz for 5 or 40 sec and measured as the amount of depolarization recorded in the B2 sniffer.

During the 5-sec stimulation (Fig. 4C), the B2 response was twofold greater when helSynKD cells were

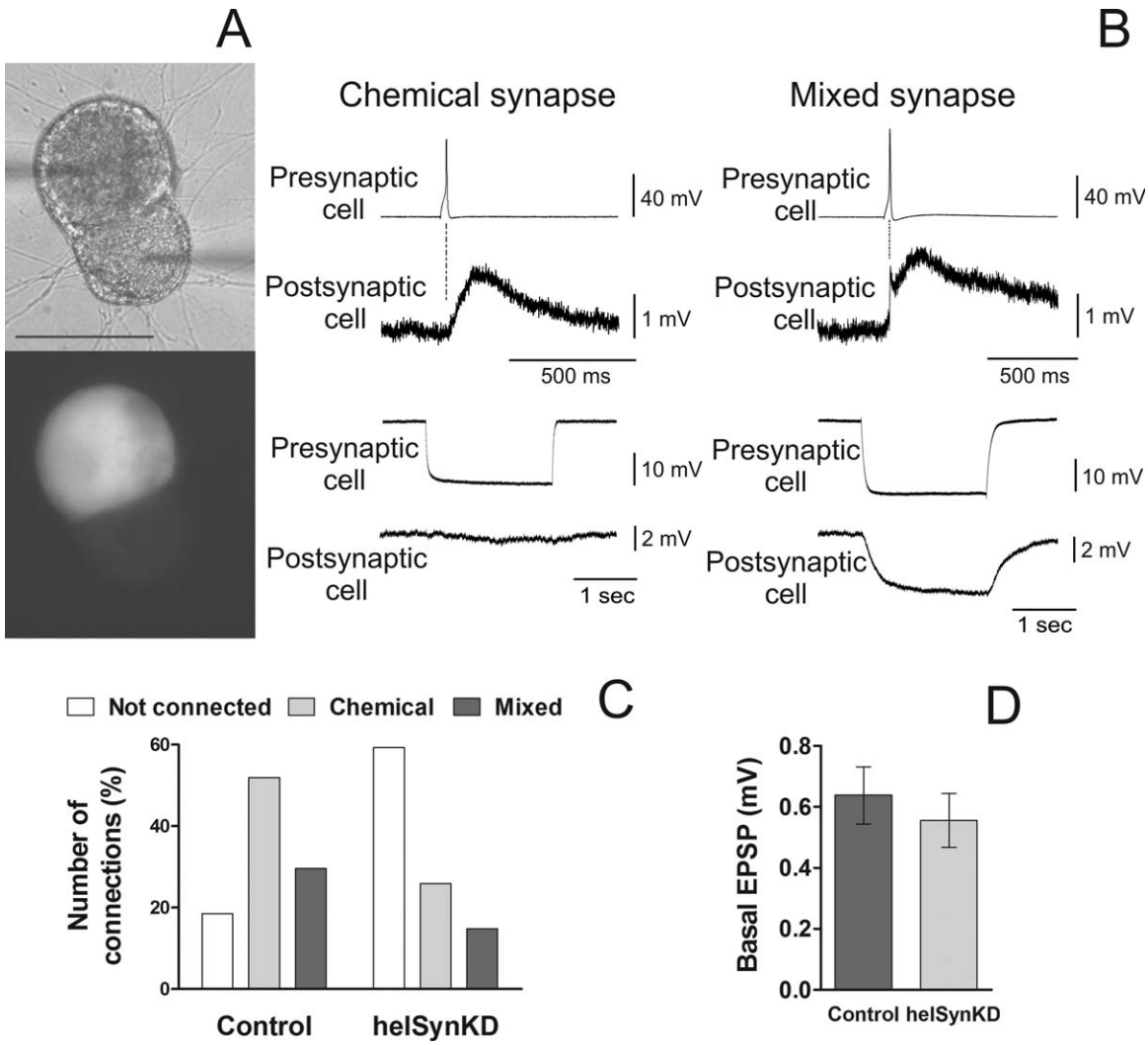

Fig. 5. Syn knockdown decreased the capacity of synapse establishment without changing basal transmission. **A:** Phase-contrast (top) and fluorescence (bottom) micrographs of a C1–B2 pair cultured in soma–soma configuration. **B:** Sample recordings of chemical (at left) and mixed (at right) C1–B2 synapse. The basal membrane potential of B2 was kept at −80 mV to prevent firing. The vertical dashed lines (at top) aligned with the peak of the presynaptic action potential show the EPSP short delay in chemical synapses and the postsynaptic corresponding peak in mixed (electrical–chemical) synapses. **C:** Occurrence of chemical and mixed connections between C1 and B2 neurons in control and Syn-deficient cells (helSynKD). **D:** Basal EPSP evoked in B2 neurons after a single presynaptic spike in control and helSynKD cells. Values represent mean ± SEM. Scale bar = 100 μm.

stimulated (10.01 ± 2.04 mV; n = 17) compared with control cells (4.45 ± 1.00 mV; n = 11; Welch-corrected t_{22} = 2.45, P = 0.023; Fig. 4D), suggesting an enhanced evoked neurotransmitter release during tetanic stimulation in the helSynKD cells. The maximal amplitude of sniffer depolarization induced by a 40-sec stimulation (Fig. 4E) in the helSynKD cells as well as in control cells was similar (13.06 ± 1.99 mV [n = 17] in helSynKD cells vs. 12.52 ± 1.95 mV [n = 11] in control cells; P = 0.853, *t*-test; Fig. 4F).

helSyn Reduction Affects the Occurrence of Chemical Synapses but Not Basal Transmission

C1 neurons (control and helSynKD) in soma configuration were coupled to B2 neurons (Fig. 5A) and recorded 48 hr later to allow synapse formation. We previously observed that, in this configuration, C1 and B2 neurons can form chemical and mixed synapses (Fig. 5B; Fiumara et al., 2005) and that the establishment of functional synapses is strongly affected by the phosphorylation state of helSyn (Giachello et al., 2010). In control cells, 81.48% of the C1–B2 pairs (n = 27) were able to generate functional synapses, 51.85% of tested pairs presented pure chemical synapses, and 29.63% presented mixed synapses. On the other hand, only 40.74% of the helSynKD cells tested (n = 27) were able to generate functional synapses with the B2 cells; 25.93% were pure chemical synapses, and 14.81% were mixed synapses (Fig. 5C). In summary, in helSynKD cells, synaptogenesis was decreased 50% vs.

control cells ($P = 0.0047$, FE test), but no significant differences were observed in the proportion of chemical and mixed connections developed by control or helSynKD cells ($P = 1.00$, FE test). In addition, no pure electrical synapses were observed in any of the cases.

In the mixed synapses, the electrical coupling was less than 10% in both control (9.99% ± 2.15%; n = 8) and helSynKD (7.09% ± 0.84%; n = 4; $P = 0.38$, *t*-test) cells. Despite the reduced occurrence of chemical synapses, the mean amplitude of the basal EPSP evoked by a single presynaptic AP was statistically similar between helSynKD and control cells (0.56 ± 0.09 mV [n = 11] in helSynKD cells vs. 0.64 ± 0.09 mV [n = 22] in control cells; $P = 0.58$, *t*-test; Fig. 5D).

helSyn Knockdown Effects on Short-Term Synaptic Plasticity

It has been shown that several *Helix* monosynaptic connections undergo different forms of short-term homosynaptic plasticity (Fiumara et al., 2005), and in some of them Syns have been involved (Cesca et al., 2010). In our model, we tested PPF, FF, and PTP. PPF was elicited with interspike intervals of 100 and 500 msec ($PPF_{100msec}$ and $PPF_{500msec}$, respectively), and FF was evoked by using short trains of five presynaptic APs at 2 Hz. The degree of facilitation was estimated as the ratio between the fifth and the first EPSP (Fiumara et al., 2005). No statistical difference was observed in $PPF_{100msec}$ (1.23 ± 0.15 [n = 10] in helSynKD cells vs. 1.00 ± 0.11 [n = 18] in control cells; $P = 0.22$, *t*-test; Fig. 6A), $PPF_{500msec}$ (1.15 ± 0.09 [n = 8] in helSynKD cells vs. 1.24 ± 0.12 [n = 14] in control cells; $P = 0.60$, *t*-test; Fig. 6B), or FF (2.18 ± 0.63 [n = 8] in helSynKD cells vs. 2.01 ± 0.30 [n = 14] in control cells; $P = 0.78$, *t*-test; Fig. 6C).

The PTP time course after a 2-sec tetanic stimulation was similar in both control and helSynKD cells (Fig. 6D, at left). The degree of potentiation was estimated as the percentage of increase in the EPSP evoked 30 sec after the tetanic stimulation, normalized to the mean of five pretrain EPSPs evoked at 0.05 Hz (Fiumara et al., 2005). We observed high variability but no statistical differences between helSynKD cells (291.3% ± 74.7%; n = 9) and control cells (253.8% ± 43.5%; n = 16; $t_{23} = 0.47$, $P = 0.64$; Fig. 6D, at right).

Faster Neurotransmitter Release in Monosynaptic Circuits

We have shown that there are no significant differences in the basal EPSPs evoked in targets of control and helSynKD cells (Fig. 5D), although a stronger neurotransmitter release is elicited by a 5-sec high-frequency stimulation in Syn-silenced isolated C1 neurons (Fig. 4C). Therefore, we tested the effect of high-frequency stimulation (a 10-Hz train of APs by 10 sec) on neurotransmitter release from C1 neurons chemically coupled to B2 neurons (Fig. 7A). The depolarization of the postsynaptic B2 neuron was measured at one-half and at the end of the train. In the first 5 sec of stimulation (one-half of the stimulation), the cells depleted of Syn evoked a stronger B2 depolarization (17.80 ± 2.43 mV; n = 11) than control cells (11.83 ± 1.60 mV; n = 19; $t_{28} = 2.14$, $P = 0.042$; Fig. 7B). Toward the end of the 10-sec stimulation, there was no statistical difference in the depolarization evoked in B2 contacting either helSynKD (12.17 ± 1.82 mV; n = 11) or control cells (12.10 ± 1.46 mV; n = 19; $P = 0.98$, *t*-test; Fig. 7C).

During the first 5 sec of stimulation, the helSynKD cells presented a stronger facilitation than control cells, as shown by the normalized EPSPs (Fig. 7D). These data agree with the neurotransmitter release estimated for the isolated C1 neurons by using sniffer B2 cells. In addition, we observed a marked rundown of the evoked EPSPs toward the end of the tetanic stimulation in the C1–B2 pairs in which Syn was silenced (Fig. 7A). This might suggest a different handling of the vesicle pools.

To estimate the total size of the RRP_{syn} and the rate of vesicle replenishment, a rapid-depletion protocol was used (Schneggenburger et al., 1999), a protocol previously used in *Helix* neurons (Giachello et al., 2013). Both cumulative profiles presented a rapid rise, followed by a slower linear increase (Fig. 7E). Because it has been demonstrated that the slow linear rise corresponds to the equilibrium between the depletion of the RRPs and their replenishment, the back-extrapolation of a fitted line to time 0 yields a rough estimate of the size of the RRP_{syn}. Syn knockdown was associated with an increase in the mean size of the RRP_{syn} from 5.81 ± 1.58 mV (n = 9) in control cells to 13.15 ± 3.16 mV (n = 8) in helSynKD cells ($t_{15} = 2.15$, $P = 0.048$; Fig. 7F). No changes in the replenishment rate of the RRP were observed because there is no statistically significant difference in the slope of the fitted lines ($P = 0.83$, *t*-test; Fig. 7G).

DISCUSSION

Syn roles in synapse genesis and function are still unclear, and different mouse models have sometimes shown conflicting results Therefore, in the present study, we describe the effects of Syn knockdown on a monosynaptic connection in vitro, reproducing a known physiological synapse.

As previously observed (Ghirardi et al., 1996; Fiumara et al., 2007; Giachello et al., 2010), helSyn presents a positive targeting to varicosities, and we show that its TF is slightly higher than that observed in human SynIb (Gitler et al., 2004a). Constitutive expression of an asRNA allowed for the long-term inhibition of helSyn synthesis, and protein levels decreased in a time-dependent manner as a function of the protein half-life, reaching up to 90% inhibition after 48–72 hr. Neurite outgrowth correlated with helSyn inhibition, and suppression of helSyn before plating resulted in a stronger negative effect on neurite elongation and branching. The role of Syn in neurite outgrowth is still unclear, mainly because experimental results are controversial. SynI-deficient mammalian neurons show neurites that elongate at a slower rate and are less branched than WT (Chin et al., 1995;

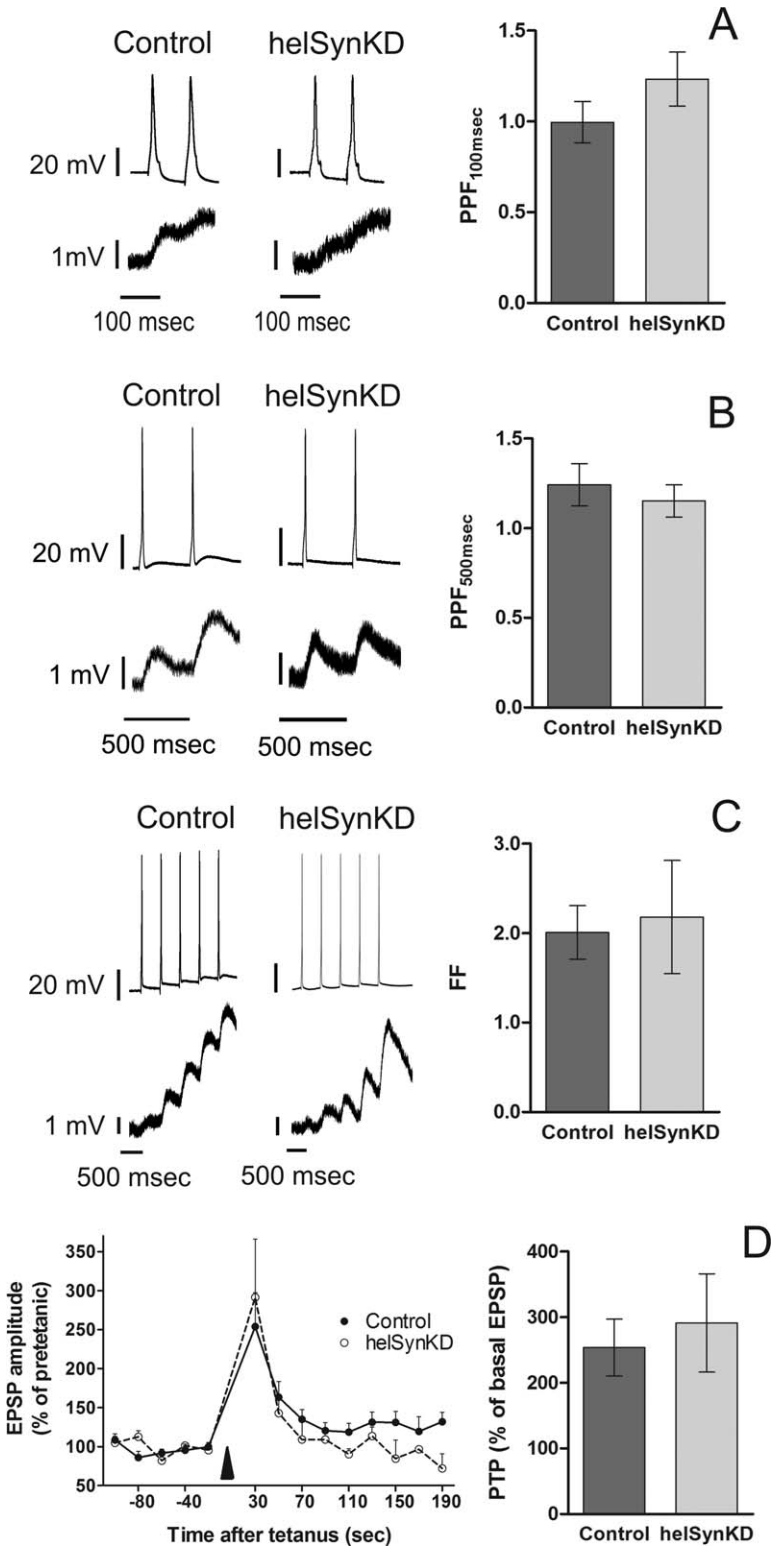

Fig. 6. Syn knockdown effects on short-term synaptic plasticity. Two presynaptic action potentials with 100-msec (**A**) and 500-msec (**B**) interspike intervals ($PPF_{100msec}$ and $PPF_{500msec}$, respectively) were used to estimate paired-pulse facilitation. **C:** Facilitation was estimated as the ratio between the fifth and the first EPSPs of a 2-Hz stimulation. Sample electrophysiological recordings are shown at left in A–C. **D:** Time course of EPSP amplitude changes in control cells and Syn-silenced cells after a 2-sec tetanic stimulation at 10 Hz are shown at left; PTP percentage was estimated 30 sec after the tetanic stimulation are shown at right. Values represent mean ± SEM.

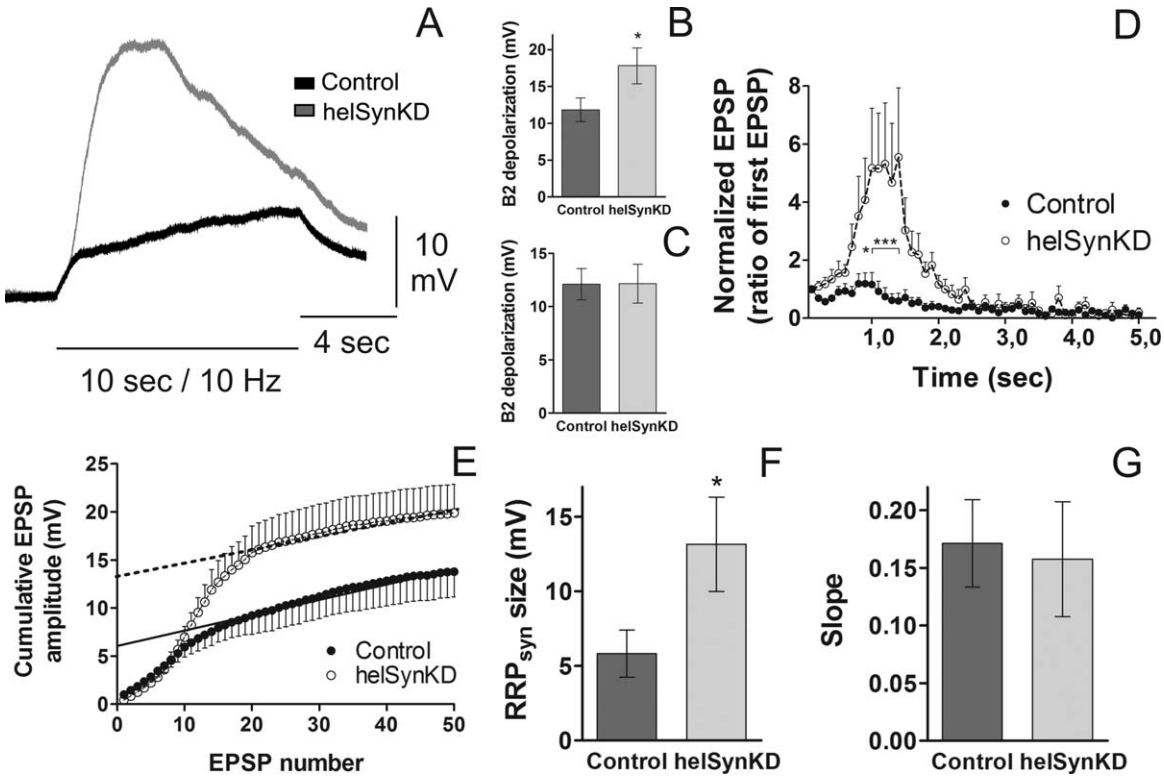

Fig. 7. Syn knockdown increased neurotransmitter release under high-frequency stimulation, changing synaptic vesicle pool constitution. **A:** Sample electrophysiological recording from B2 postsynaptic cell during a tetanic stimulation (horizontal bar) in C1 control and Syn-depleted cells (helSynKD). **B:** B2 depolarization amplitude at half recording. **C:** B2 depolarization amplitude at the end of the recording. **D:** Plot of the EPSPs (normalized against the first EPSP of the tetanus) during the first 5 sec of stimulation. **E:** Cumulative EPSP amplitude profiles. To estimate the size of RRP_{syn}, data points were fitted by linear regression from the last point and back-extrapolated to T0 in control (solid circles) and helSynKD (open circles) cells. **F:** Graph of the estimated RRP_{syn} size. **G:** Slopes of the fitted lines as an estimate of vesicle replenishment rates. Values represent mean ± SEM. $\star P < 0.05$, $\star\star\star P < 0.001$.

Ferreira et al., 1998). SynII-deficient neurons are unable to elongate their processes, or they develop short, undifferentiated neurites (Ferreira et al., 1994, 1998). Moreover, neurons lacking SynIII fail to elongate axons (Ferreira et al., 2000). However, Syn double- and triple-KO models show an absence of the deleterious effects of each individual deletion, and neurite development is largely restored (Ferreira et al., 1998; Valtorta et al., 2011). The likely explanation is the occurrence of compensatory mechanisms developed when two or three Syn genes are deleted (Rosahl et al., 1995). We could not exclude the presence of compensatory mechanisms in helSynKD cells when we suppressed Syn synthesis with the asRNA; however, the robust decrease in neurite elongation and branching strongly supports the important role of Syn in neurite development.

We also show a remarkable decrease in number and size of presynaptic varicosities in helSynKD cells, and the number of functional connections developed between pairs of C1–B2 neurons was decreased 50% on these cells. These data agree with reports of previous studies in which the manipulation of Syn phospho levels decreased the formation of functional connections between *Helix* neurons (Giachello et al., 2010) and support the proposed role of Syns in the formation and stabilization of synapses (Cesca et al., 2010).

We observed a 40% decrease in the total number of varicosities when the helSynKD cells were plated with their original axons and a stronger decrease (84%) when cells were plated in soma configuration, which represents an extreme condition for cell outgrowth. These results could be consistent with the 70% decrease in synapse formation quantified by using synaptophysin-immunoreactive spots after SynII suppression with asRNA (Ferreira et al., 1995) or the less intense decrease of 28% observed in glutamatergic synapses from cells treated with SynI small-interference RNA (Perlini et al., 2011) and highlight the important role of Syn proteins in the establishment of synapses.

Actin cytoskeleton dynamics are associated with elongation and branching of neurites, generation of varicosities, and formation and stabilization of synapses (Cesca et al., 2010; Schmidt and Rathjen, 2010; Gallo, 2011; Stiess and Bradke, 2011; Giachello et al., 2012). Moreover, it is known that Syn produces actin nucleation and participates in cytoskeleton structure, interacting with spectrin, tubulin, annexin, calmodulin, lipids, and neurofilaments

(Cesca et al., 2010). Therefore, it is possible that Syn inhibition creates cytoskeleton alterations associated with aberrant growth, fewer and smaller varicosities, and decreased synapse stabilization.

We tested the amplitude of the excitatory postsynaptic potentials (EPSPs) evoked by control cells and Syn-silenced cells, and no differences were observed. EPSPs are determined by variables such as the number of releasing sites (N) and the probability of vesicle release (P_r; Schneggenburger et al., 2002). In helSynKD cells, we observed a reduction in varicosity number, which may indicate a smaller N, without detectable changes in the basal EPSP amplitude. This apparent discordance could be associated with an increased P_r in helSynKD cells. Several authors have proposed that P_r is dependent on a balance between two processes, the probability of release, which is dependent on calcium currents, and the size of the RRP (Saviane et al., 2002), expressed as $P_r = P_r(Ca^{2+}) \times P_r(Ves)$.

The interplay between these processes at the moment of arrival of each spike would determine the EPSP amplitude and the presence of facilitation or depression (Saviane et al., 2002). Our results indicate an increased RRP_{syn} in helSynKD cells vs. control cells, possibly reflecting an increased vesicle availability [$\uparrow P_r(Ves)$] and subsequent increase in P_r, which could compensate for the decrease in N, evoking similar single EPSPs as observed in control cells. To characterize these results better, we are also currently studying the possible changes in Ca^{2+} currents and quantal size.

In addition to the increased RRP, we also observed a decreased capacity for maintaining NT release for long periods of high-frequency activity (10 sec at 10 Hz). From these results, we can infer the likely events occurring during tetanic stimulation (Fig. 8). In control cells, a single AP evoked the release of a small fraction of the RRP (Reyes et al., 1998; Schneggenburger et al., 1999), leading to a mean EPSP of 0.64 mV from an estimated RRP_{syn} of 5.81 mV. At high-frequency stimulation, the continuous spiking activity increases the residual Ca^{2+} [$\uparrow P_r(Ca^{2+})$], thus promoting the release of more vesicles from the RRP until depletion. Afterward, the control cells are able to keep their postsynaptic targets depolarized (Figs. 7A [black record], 8A).

Conversely, in helSynKD cells, the increased NT release at the beginning of the stimulation and the subsequent decrease in the postsynaptic response suggest an impairment in the handling of the vesicle pools (Fig. 7A, gray record). When Syn is silenced (Fig. 8B), it is possible that SV from the reserve pool (RP) gains a higher mobility (Orenbuch et al., 2012), compromising RP size and increasing RRP (estimated RRP_{syn} = 13.15 mV). An increased $P_r(Ves)$ could allow a basal EPSP amplitude (0.56 mV) comparable to that of control cells. During high-frequency stimulation, the increased RRP and $P_r(Ves)$ induce the release of an increased number of vesicles, evoking a stronger B2 response until the RRP depletion (Fig. 7A). Subsequently, a compromised RP could be related to synaptic fatigue and decrease in the postsynaptic response in the second half of the 10-sec tetanus.

Our model is consistent with TKO mouse models described in the literature in which a similar excitatory postsynaptic current amplitude (Gitler et al., 2004b), increased RRP (Kile, 2010; Farisello et al., 2013), decreased RP (Gitler et al., 2004b; Orenbuch et al., 2012), and increased SV mobility (Orenbuch et al., 2012) vs. WT mice has been reported. In addition, the decreased RP is one of the features observed in most single-, double-, and triple-KO models (except for SynIII KO; Cesca et al., 2010).

Several authors have observed a decreased total number of SV in excitatory synapses of TKO mice (Gitler et al., 2004b; Siksou et al., 2007; Cesca et al., 2010; Orenbuch et al., 2012), but this apparently discordant data could be explained by the increased vesicle mobility, which can induce movement of SV outside the presynaptic terminal, decreasing the total number of SVs observed in this structure via electron microscopy but probably increasing the pool of vesicles localized in the axons (axonal pool; Denker and Rizzoli, 2010; Orenbuch et al., 2012). These SVs could be released during high-frequency stimulation only if the accumulation of residual Ca^{2+} is strong enough for their recruitment, increasing $Pr(Ca^{2+})$. Taken together, these data strongly support the role of Syns in the establishment of the vesicle pools and their role in the maintenance of neuron capacity to maintain SV exocytosis under high-frequency stimulation, regulating the constant resupply of SVs.

With respect to the role of Syn in short-term synaptic plasticity, we observed no significant differences in paired-pulse facilitation with different ISIs or frequency facilitation. Similar results were reported by Fiumara et al. (2007) in that the overexpression of either helSyn WT or a nonphosphorylatable mutant does not affect frequency facilitation. In the literature, there is evidence that Syn is implicated in PTP both from mammal (Farisello et al., 2013) and from invertebrate (Humeau et al., 2001) models. For *Helix*, we previously reported that preventing helSyn phosphorylation is sufficient to impair PTP (Fiumara et al., 2007; Giachello et al., 2010). Here, we find no statistical differences in the degree of potentiation in helSynKD cells, although the same induction protocol was applied (2 sec at 10 Hz, as described by Fiumara et al., 2007). One possibility is that the presynaptic overexpression of a nonphosphorylatable Syn mutant acts in a dominant-negative manner by affecting vesicle clustering and severely impairing PTP. This may suggest that the interconversion cycle of dephosphorylated–phosphorylated Syn rather than protein abundance is more relevant for PTP expression. Another possibility that we cannot exclude is that the mechanism underlying PTP induction is different in control cells and Syn-silenced cells. We previously showed that inhibitors of calmodulin kinase and protein kinase A impair PTP in C1–B2 synapses (Fiumara et al., 2007); future studies are required to determine whether PTP induction in helSynKD cells is similarly affected by these inhibitors.

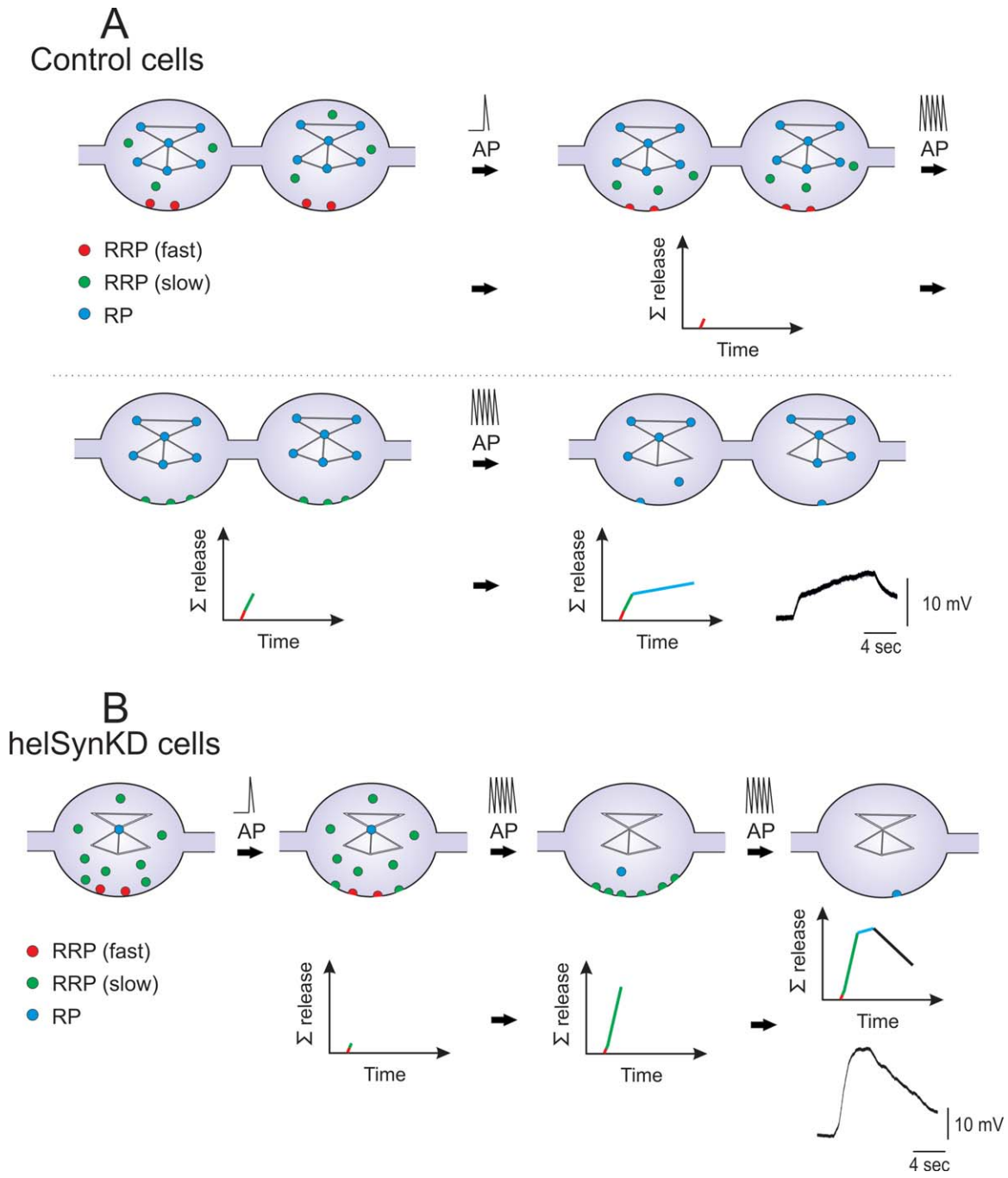

Fig. 8. Vesicle release under high-frequency stimulation in control and Syn-knockdown cells (helSynKD). **A:** In control cells, upon arrival of the first AP, the releasable fraction of the fast RRP is released. Further stimulation results in the release of the rest of the RRP (slow RRP). When stimulation continues, the RP is recruited. **B:** In helSynKD cells, there are fewer varicosities, the RRP is increased with highly mobile vesicles, and the RP is compromised. The first AP leads to the release of more synaptic vesicles than in control cells (slow and fast vesicles). Further stimulation evoked increased release of almost all the vesicles, leading to a strong decrease in the postsynaptic response when the stimulation was continuous. The lower panels (Σ release) indicate the neurotransmitter release against time and at the end postsynaptic recordings obtained during stimulation of controls, and helSynKD cells are shown as **insets**.

It has also been suggested that PTP impairment could be associated with a depletion of the RP and RRP exhaustion during the conditioning stimulus, which cannot be replenished when the PTP is tested (Humeau et al., 2001). Another possibility is the incomplete RRP depletion during the 2-sec conditioning stimulus or a

faster RRP replenishment between the tetanus and the resumed basal stimulation.

In summary, we used a simple monosynaptic model in which Syn protein was knocked down in the presynaptic terminals, and the results of our experiments highlight the important role of Syns in the development of neurites and in the formation of varicosities. This study shows that the development of functional synapses is not dependent solely on Syn phosphorylation status, as previously indicated, but is also dependent on the correct expression of Syn proteins. Our results underscore the importance of Syn in the assembly and maintenance of SV pools, thus affecting the RRP size and the capacity of the cell to respond to high-frequency stimulation by tuning synaptic vesicle availability.

ACKNOWLEDGMENTS

The authors thank Virginia Eterno and Andrea Cerase for their technical support; Ferdinando Fiumara for technical support, manuscript correction, and helpful comments; Adarli Romero for helpful comments; and Paul Hanson for language correction.

CONFLICT OF INTEREST STATEMENT

The authors have no actual or potential conflicts of interest, including any financial, personal, or other relationships with people or organizations that could influence the present article.

ROLE OF AUTHORS

The experiments included in this study were performed and the manuscript was written mainly by OB. CNGG participated in experiment planning, analysis, and valuable discussion. PGM and MG participated in experiment planning and discussion. All authors participated in manuscript correction.

REFERENCES

Cesca F, Baldelli P, Valtorta F, Benfenati F. 2010. The synapsins: key actors of synapse function and plasticity. Prog Neurobiol 91:313–348.

Chiappalone M, Casagrande S, Tedesco M, Valtorta F, Baldelli P, Martinoia S, Benfenati F. 2009. Opposite changes in glutamatergic and GABAergic transmission underlie the diffuse hyperexcitability of synapsin I-deficient cortical networks. Cereb Cortex 19:1422–1439.

Chin LS, Li L, Ferreira A, Kosik KS, Greengard P. 1995. Impairment of axonal development and of synaptogenesis in hippocampal neurons of synapsin I-deficient mice. Proc Natl Acad Sci U S A 92:9230–9234.

Corradi A, Fadda M, Piton A, Patry L, Marte A, Rossi P, Cadieux-Dion M, Gauthier J, Lapointe L, Mottron L, Valtorta F, Rouleau GA, Fassio A, Benfenati F, Cossette P. 2014. SYN2 is an autism predisposing gene: loss-of-function mutations alter synaptic vesicle cycling and axon outgrowth. Hum Mol Genet 23:90–103.

Denker A, Rizzoli SO. 2010. Synaptic vesicles pools: an update. Front Synaptic Neurosci 2:135. doi:10.3389/fnsyn.2010.00135.

Farisello P, Boido D, Nieus T, Medrihan L, Cesca F, Valtorta F, Baldelli P, Benfenati F. 2013. Synaptic and extrasynaptic origin of the excitation/inhibition imbalance in the hippocampus of synapsin I/II/III knockout mice. Cereb Cortex 23:581–593.

Fassio A, Patry L, Congia S, Onofri F, Piton A, Gauthier J, Pozzi D, Messa M, Defranchi E, Fadda M, Corradi A, Baldelli P, Lapointe L, St-Onge J, Meloche C, Mottron L, Valtorta F, Nguyen DK, Rouleau GA, Benfenati F, Cossette P. 2011. SYN1 loss-of-function mutations in autism and partial epilepsy cause impaired synaptic function. Hum Mol Genet 20:2297–2307.

Feng J, Chi P, Blanpied TA, Xu Y, Magarinos AM, Ferreira A, Takahashi RH, Kao HT, McEwen BS, Ryan TA, Augustine GJ, Greengard P. 2002. Regulation of neurotransmitter release by synapsin III. J Neurosci 22:4372–4380.

Ferreira A, Kosik KS, Greengard P, Han HQ. 1994. Aberrant neurites and synaptic vesicle protein deficiency in synapsin II-depleted neurons. Science 264:977–979.

Ferreira A, Han HQ, Greengard P, Kosik KS. 1995. Suppression of synapsin II inhibits the formation and maintenance of synapses in hippocampal culture. Proc Natl Acad Sci U S A 92:9225–9229.

Ferreira A, Chin LS, Li L, Lanier LM, Kosik KS, Greengard P. 1998. Distinct roles of synapsin I and synapsin II during neuronal development. Mol Med 4:22–28.

Ferreira A, Kao HT, Feng J, Rapoport M, Greengard P. 2000. Synapsin III: developmental expression, subcellular localization, and role in axon formation. J Neurosci 20:3736–3744.

Fiumara F, Onofri F, Benfenati F, Montarolo PG, Ghirardi M. 2001. Intracellular injection of synapsin I induces neurotransmitter release in C1 neurons of *Helix pomatia* contacting a wrong target. Neuroscience 104:271–280.

Fiumara F, Giovedì S, Menegon A, Milanese C, Merlo D, Montarolo PG, Valtorta F, Benfenati F, Ghirardi M. 2004. Phosphorylation by cAMP-dependent protein kinase is essential for synapsin-induced enhancement of neurotransmitter release in invertebrate neurons. J Cell Sci 117:5145–5154.

Fiumara F, Leitinger G, Milanese C, Montarolo PG, Ghirardi M. 2005. In vitro formation and activity-dependent plasticity of synapses between *Helix* neurons involved in the neural control of feeding and withdrawal behaviors. Neuroscience 134:1133–1151.

Fiumara F, Milanese C, Corradi A, Giovedi S., Leitinger G., Menegon A., Montarolo PG, Benfenati F, Ghirardi M. 2007. Phosphorylation of synapsin domain A is required for posttetanic potentiation. J Cell Sci 120:3228–3237.

Gaffield MA, Betz WJ. 2007. Synaptic vesicles mobility in mouse motor nerve terminals with and without synapsin. J Neurosci 27:13691–13700.

Gallo G. 2011. The cytoskeletal and signaling mechanisms of axon collateral branching. Dev Neurobiol 71:201–220.

Garcia CC, Blair HJ, Seager M, Coulthard A, Tennant S, Buddles M, Curtis A, Goodship JA. 2004. Identification of a mutation in synapsin I, a synaptic vesicle protein, in a family with epilepsy. J Med Genet 41: 183–186.

Ghirardi M, Casadio A, Santarelli L, Montarolo PG. 1996. *Aplysia* hemolymph promotes neurite outgrowth and synaptogenesis of identified *Helix* neurons in cell culture. Invert Neurosci 2:41–49.

Ghirardi M, Naretto G, Fiumara F, Vitiello F, Montarolo PG. 2001. Target-dependent modulation of neurotransmitter release in cultured *Helix* neurons involves adhesion molecules. J Neurosci Res 65:111–120.

Giachello CNG, Fiumara F, Giacomini C, Corradi A, Milanese C, Ghirardi M, Benfenati F, Montarolo PG. 2010. MAPK/Erk-dependent phosphorylation of synapsin mediates formation of functional synapses and short-term homosynaptic plasticity. J Cell Sci 123:881–893.

Giachello CNG, Montarolo PG, Ghirardi M. 2012. Synaptic functions of invertebrate varicosities: what molecular mechanisms lie beneath. Neural Plast 2012:670821.

Giachello CNG, Premoselli F, Montarolo PG, Ghirardi M. 2013. Pentylenetetrazol-induced epileptiform activity affects basal synaptic transmission and short-term plasticity in monosynaptic connections. PloS One 8:e56968.

Gitler D, Xu Y, Kao HT, Lin D, Lim S, Feng J, Greegard P, Augustine G. 2004a. Molecular determinants of synapsin targeting to presynaptic terminals. J Neurosci 24:3711–3720.

Gitler D, Takagishi Y, Feng J, Ren Y, Rodriguez RM, Wetsel WC, Greengard P, Augustine GJ. 2004b. Different presynaptic roles of synapsins at excitatory and inhibitory synapses. J Neurosci 24:11368–11380.

Greco B, Managò F, Tucci V, Kao HT, Valtorta F, Benfenati F. 2013. Autism-related behavioral abnormalities in synapsin knockout mice. Behav Brain Res 251:65–74.

Humeau Y, Doussau F, Vitiello F, Greengard P, Benfenati F, Poulain B. 2001. Synapsin controls both reserve and releasable synaptic vesicle pools during neuronal activity and short-term plasticity in *Aplysia*. J Neurosci 21:4195–4206.

Kile BM, Guillot TS, Venton BJ, Wetsel WC, Augustine GJ, Wightman RM. 2010. Synapsins differentially control dopamine and serotonin release. J Neurosci 30:9762–9770.

Medrihan L, Cesca F, Raimondi A, Ligani G, Baldelli P, Benfenati F. 2013. Synapsin II desynchronizes neurotransmitter release at inhibitory synapses by interacting with presynaptic calcium channels. Nat Commun 4:1512.

Orenbuch A, Shalev L, Marra V, Sinai I, Lavy Y, Kahn J, Burden JJ, Staras K, Gitler D. 2012. Synapsin selectively controls the mobility of resting pool vesicles at hippocampal terminals. J Neurosci 32:3969–3980.

Perlini LE, Botti F, Fornasiero EF, Giannandrea M, Bonanomi D, Amendola M, Naldini L, Benfenati F, Valtorta F. 2011. Effects of phosphorylation and neuronal activity on the control of synapse formation by synapsin I. J Cell Sci 124:3643–3653.

Reyes A, Lujan R, Rozov A, Burnashev N, Somogyi P, Sakman B. 1998. Target-cell-specific facilitation and depression in neocortical circuits. Nat Neurosci 1:279–285.

Rosahl TW, Spillane D, Missler M, Herz J, Selig DK, Wolff JR, Hammer RE, Malenka RC, Sudhof TC. 1995. Essential functions of synapsin-I and synapsin-II in synaptic vesicle regulation. Nature 375:488–493.

Saviane C, Savtchenko LP, Raffaelli G, Voronin LL, Cherubini E. 2002. Frequency-dependent shift from paired-pulse facilitation to paired-pulse depression at unitary CA3–CA3 synapses in the rat hippocampus. J Physiol 544:469–476.

Schmidt H, Rathjen FG. 2010. Signalling mechanisms regulating axonal branching in vivo. Bioassays 32:977–985.

Schneggenburger R, Meyer AC, Neher E. 1999. Released fraction and total size of a pool of immediately available transmitter quanta at a calyx synapse. Neuron 23:399–409.

Schneggenburger R, Sakaba T, Neher E. 2002. Vesicle pools and short-term synaptic depression: lessons from a large synapse. Trends Neurosci 25:206–212.

Siksou L, Rostaing P, Lechaire JP, Boudier T, Ohtsuka T, Fejtová A, Kao HT, Greengard P, Gundelfinger ED, Triller A, Marty S. 2007. Three-dimensional architecture of presynaptic terminal cytomatrix. J Neurosci 27:6868–6877.

Stiess M, Bradke F. 2011. Neuronal polarization: the cytoskeleton leads the way. Dev Neurobiol 71:430–444.

Valtorta F, Pozzi D, Benfenati F, Fornasiero EF. 2011. The synapsins: Multitask modulators of neuronal development. Semin Cell Dev Biol 22:378–386.

Washbourne P, Dityatev A, Scheiffele P, Biederer T, Weiner JA, Christopherson KS, El-Husseini A. 2004. Cell adhesion molecules in synapse formation. J Neurosci 24:9244–9249.